*Electronic Research Archive*

https://www.aimspress.com/journal/era

ERA, 33(10): 6418–6444.
DOI: 10.3934/era.2025283
Received: 11 August 2025
Revised: 07 October 2025
Accepted: 22 October 2025
Published: 29 October 2025

*Research article*

# Numerical simulation of novel stimulation strategies in the modulation of absence seizures based on an improved BGCT model

**Zhihui Wang, Yaqi Yang and Lixia Duan***

College of Science, North China University of Technology, Beijing 100144, China

* **Correspondence:** Email: duanlx@ncut.edu.cn.

**Abstract:** An absence seizure is a common neurological disorder primarily associated with abnormal interactions between the corticothalamic network and the basal ganglia. In order to better understand how the basal ganglia contributes to absence seizure regulation, we use an improved mean field model of the basal ganglia-corticothalamo (BGCT) by introducing a direct projection from the glutamatergic mediated subthalamic nucleus to the striatum (STN-D). The results indicate that enhancing the excitatory coupling strength of the STN-D pathway significantly suppresses spike-wave discharges (SWDs) by increasing striatal activation levels, which promotes the transition from the pathological state to either simple oscillations or low firing state. We propose a new stimulation paradigm, namely a four-phase pulse stimulation (FPS), which sequentially delivers four pulses to the striatum (D), thus targeting the cortical excitatory neurons (EPN), specific relay nuclei (SRN), STN, and D. The results indicate that FPS can successfully replace the original inputs to the D and effectively control absence seizures by adjusting the anodal pulse amplitudes ($A_1$, $A_2$, and $A_3$), which correspond to the excitatory inputs to the D from SRN-D, EPN-D, and SRN-D. These findings offer new insights into understanding the pathophysiology of an absence seizure and its precise therapeutic interventions.

**Keywords:** absence seizures; mean-field model; spike-wave discharges; STN-D pathway; four-phase pulse stimulation

## 1. Introduction

An absence seizure is a common neurological condition marked by short episodes of unconsciousness, especially affecting children's well-being. These nonconvulsive episodes are typically associated with bilaterally synchronous spike-wave discharges (SWDs) at 2 to 4 Hz, as recorded on electroencephalograms (EEG). This characteristic is a crucial indicator for diagnosis [1]. Numerous studies showed that absence seizures are caused by irregular activities in the cortex and thalamus [2,3]. Roberts et al. highlighted the critical role of corticothalamic and thalamocortical conduction delays in

shaping SWDs, using a physiologically grounded mean-field model of absence seizures [4]. Rodrigues et al. used a corticothalamic mean-field model to explain the transition from the interictal activity to spikes and waves in absence seizures as a result of the Hopf bifurcation [5]. However, to clearly distinguish the "origin" of rhythmicity from the "regulatory" influence of other network components, evidence from isolated thalamocortical slices is crucial. Tancredi et al. showed that the cortico-thalamic-cortical circuit has an intrinsic capacity to generate epileptiform rhythms, where applying a channel blocker (4-AP) induced spindle-like oscillations that resembled absence seizures [6]. Using brain slices from a rat model of hereditary absence seizures, D'Arcangelo et al. further discovered that the cortico-thalamic-cortical circuit generates a specific, highly synchronized slow oscillation, which confirmed its dependence on cortical N-methyl-D-aspartate (NMDA) receptor mechanisms [7]. Thus, the cortico-thalamic-cortical circuit acts as the "engine" for absence seizures, while other brain regions (e.g., basal ganglia, brainstem) may play crucial regulatory roles in initiating, sustaining, or terminating this "engine" through ascending or descending projections. In addition, physiological experimental and computer simulation studies showed that the basal ganglia plays an active role in the control of absence seizures [8–15]. According to the biophysical mean-field model of the basal ganglia-corticothalamo (BGCT) network, Chen et al. found that the basal ganglia can regulate absence seizures induced by abnormal cortical-thalamic activity in both directions [9]. Subsequent studies indicated that the basal ganglia may also send direct projections to the cerebral cortex through an additional efferent route. For example, anatomical studies revealed that the basal ganglia sends gamma-aminobutyric acid (GABA)ergic projections directly to the frontal cortex, thus implying a more direct role in modulating the cortical activity [16]. Based on the experimental basis, Chen et al. demonstrated the direct inhibitory effect of the lobus pallidus externus (GPe)-cortex pathway in absence seizures by numerical simulations with a BGCT mean-field model [17]. The modeling work by Chen et al. confirmed that the GPe can bidirectionally regulate absence seizures through its projections to the thalamic reticular nucleus (TRN), thus establishing the GPe-TRN pathway as a key regulatory hub [18]. Recent work by Hu et al. revealed that the basal ganglia modulates thalamocortical network activity via the striato-cortical pathway, which may underlie the mechanisms of absence seizures, thus suggesting striatal neurons as potential targets for therapeutic deep brain stimulation (DBS) [19]. Wang et al. showed that somatostatin (SST)/parvalbumin (PV)-mediated inhibition of pyramidal neurons regulates the speed-accuracy trade-off in motor selection [20], while excessive PV inhibition mechanistically resembles basal ganglia dysfunction in absence seizures. These findings underscore the critical role played by basal ganglia outputs in regulating absence seizures. Building on this, we improve the BGCT model to explore how specific pathways within the basal ganglia circuit influence the emergence and suppression of SWDs.

The basal ganglia primarily consist of subcortical nuclei, including the striatum (D), subthalamic nucleus (STN), and globus pallidus externus (GPe), which send axonal projections to the cortex and thalamus. Among these, the D and STN are considered the primary input nuclei of the basal ganglia. Meanwhile, the D and STN also interact with other basal ganglia nuclei. Saunders et al. demonstrated that the GPe project to both the STN and striatal interneurons, thus indicating a structural link between the indirect and hyperdirect basal ganglia pathways [21]. Fan and Wang introduced autaptic connections within the STN into a BGCT mean-field model and showed that the autaptic connection to the STN can suppress SWDs [11]. Recent studies provided evidence that glutamatergic STN neurons can directly influence the dynamical activity of the D through

their innervation of GABAergic parvalbumin-expressing interneurons [22]. This projection not only contributes to information transmission and processing within the basal ganglia, but also modulates the excitation-inhibition balance of the cortico-thalamic circuit by influencing striatal activity. It remains to be investigated whether this pathway can play a modulatory role in absence seizures.

Pharmacological intervention is one of the primary approaches for treatment [23]; however, some patients may develop resistance to antiepileptic drugs [24]. In addition, lesion resection surgery can be considered as a treatment option, but it carries significant risks. In recent years, DBS has been widely applied to treat neurological disorders [25–27]. High-frequency DBS of the STN is widely recognized as an effective therapeutic approach for Parkinson's disease, primarily through continuous high-frequency stimulation that suppresses abnormal neural activity [28, 29]. Electrophysiological studies and clinical trials demonstrated that specific stimulation paradigms can effectively suppress or control absence seizures and other neurological disorders. Fan et al. developed a simplified corticothalamic (SCT) model and found that the application of single-pulse alternately resetting stimulation (SARS) to corticothalamic circuits improved the control of absence seizures [30]. Using a modified Jansen–Rit neural mass model, Haghighi et al. demonstrated that high-frequency stimulation can effectively suppress seizures; they further demonstrated that a closed-loop stimulation strategy significantly reduces the control effort compared to continuous open-loop stimulation [31]. Bethany et al. optimized the electrical stimulation parameters such as stimulation charge, frequency, and pulse width in a data-driven manner, and found that setting the parameters correctly resulted in an improved seizure suppression [32]. Recent computational modeling studies demonstrated that electromagnetic induction can effectively assist the SRN-STN projection in suppressing SWDs, while simultaneously reducing the side effects associated with electrical stimulation [33]. Hou et al. introduced a tri-phase delay stimulation (TPDS) protocol that targeted the internal globus pallidus (GPi) in a simplified GCT model. They showed that an appropriately tuned TPDS can replicate and suppress SWDs, even under simulated blockage of the basal ganglia input pathways, thus suggesting a potential surrogate strategy for seizure control [34]. He et al. employed a bi-layered ring network model to successfully couple microscopic neuronal activity with macroscopic cortical spreading depression (CSD) propagation dynamics, thus providing novel computational evidence for the pathomechanisms underlying epilepsy-migraine comorbidity [35]. Zhao et al. demonstrated that inhibiting GABA uptake (Vgai) in cortical astrocytes can effectively control absence seizures induced by various triggers [36], thus providing a dynamical foundation for glia-targeted antiepileptic strategies. In summary, we find great potential feasibility in applying the optimized stimulation strategy to the treatment of absence seizures, which is the central focus of the present study.

In this study, we improve the BGCT mean-field model while incorporating the STN-D connection into the model on the basis of physiological experiments in order to systematically investigate the critical role of the newly discovered glutamatergic STN-D direct projections in the control of absence seizures. In addition, we propose a new stimulation strategy of four-phase pulse stimulation (FPS) to the basal ganglia to explore the effectiveness of this stimulation in modulating absence seizures. This paper is organized as follows: Section 2 describes our improved mean-field model of the basal ganglia cortical thalamus and the analytical approach and model parameters of this paper; Section 3 analyzes the critical role of the newly added direct STN-D projection in controlling SWDs during absence seizures, while also examining how the other three direct striatal input pathways (EPN-D, SRN-D and D-D) contribute to SWDs regulation; in Section 4, we propose a new stimulation paradigm that

models the physiological dynamics of excitatory and inhibitory inputs to explore its potential as an alternative striatal regulatory mechanism and its effectiveness in suppressing absence seizures; through a two-parameter state analysis, we determine the range of effects of key parameters on the model state and also explore the limitations of this stimulation modality; and finally, we summarize the results of the study.

## 2. Materials and methods

### 2.1. The model structure

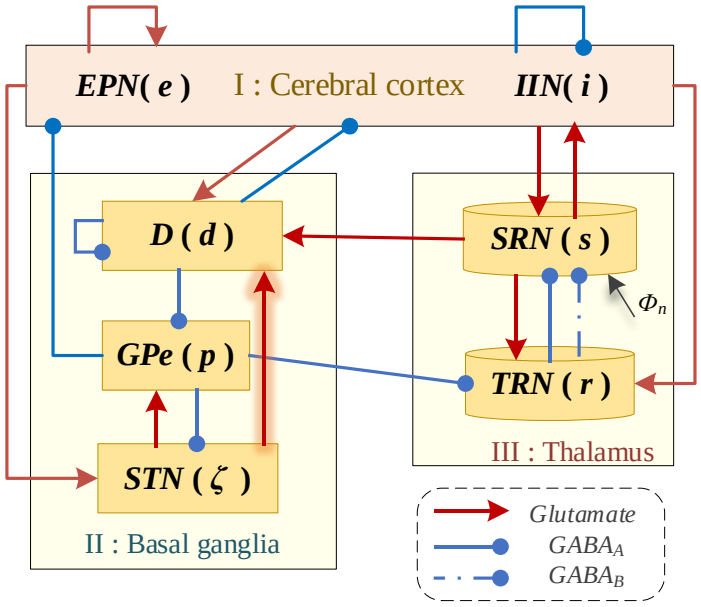


**Figure 1.** Schematic diagram of the improved BGCT model. The BGCT network framework consists of cortical, thalamic, and basal ganglia subnetworks. The cortical subnetwork includes excitatory pyramidal neurons ( $e$ ) and inhibitory interneurons ( $i$ ), the thalamic subnetwork consists of the TRN ( $r$ ) and the SRN ( $s$ ), and the basal ganglia subnetwork consists of the striatum ( $d$ ), GPe ( $p$ ), and the STN ( $\zeta$ ). Red arrows represent glutamate-mediated excitatory projections, while solid and dashed blue lines with circular ends indicate $GABA_A$ and $GABA_B$ mediated inhibitory projections, respectively. $\phi_n$ is the nonspecific external input to the SRN.

To better understand how the BGCT network regulates absence seizures, we improve on the biophysical model proposed by Chen et al. [9], which still maintains simplicity and is centralised. To fully explore the role of the D, we combine $D_1$ and $D_2$ striatal neurons to analyze the overall activity of the D. The substantia nigra pars reticulata (SNr) is not the main area involved in absence seizures or other brain disorders [37]. Existing research indicates that the GPe also serves as a crucial output nucleus within the basal ganglia, with its pathway to the thalamus that plays a key role in suppressing absence seizures. In our investigation, simplifying the SNr nucleus does not affect the output from the basal ganglia to the thalamic circuit via GPe [18]. Because of this, we remove the SNr from the

model and mainly focus on the three key nuclei: D, GPe, and STN, which are primarily connected to the cortico-thalamic network. Removing SNr neurons from the model and incorporating $D_1$ and $D_2$ striatal neurons not only simplifies the model, but also does not change the main understanding of how these three nuclei affect absence seizures.

The improved BGCT network consists of seven neuronal populations (Figure 1). The cortex is composed of pyramidal cells with excitatory properties (EPN) and inhibitory interneurons (IIN), whereas the thalamus contains the TRN and SRN. The cortico-thalamic system is formed by the interaction of EPN, IIN, TRN, and SRN. The basal ganglia region includes the D, GPe, and STN. For convenience in subsequent descriptions, these neuronal populations are abbreviated as $e$ (EPN), $i$ (IIN), $r$ (TRN), $s$ (SRN), $d$ (D), $p$ (GPe), and $\zeta$ (STN). The BGCT network contains three types of neural projections. For clarity, different types of lines and labels are used to distinguish them (Figure 1). Red arrows represent glutamate-mediated excitatory projections, while solid and dashed blue lines with circular ends indicate $GABA_A$ and $GABA_B$ mediated inhibitory projections, respectively. The connectivity between different neuronal populations is primarily inspired by previous modeling studies. In addition, it is hypothesized that the SRN is subjected to a steady external excitatory sensory drive, denoted as $\phi_n$.

### *2.2. The mean-field equation*

The activity of a population of neurons is described by a mean-field model, which simplifies the study of the overall behavior of neural populations. It is computationally efficient and effective, as shown in previous studies [9]. The initial component of the model emphasizes how neuronal populations respond, on average, to variations in their somatic membrane potential. For each group of neurons, the average firing rate $Q_a$ depends on the mean membrane potential $V_a$, following a sigmoidal function:

$$Q_a(t) \equiv S[V_a(t)] = \frac{Q_a^{\max}}{1 + \exp\left[-\frac{\pi}{\sqrt{3}}\frac{(V_a(t)-\theta_a)}{\sigma}\right]}, \tag{2.1}$$

where $a \in A = \{e, i, r, s, d, p, \zeta\}$, identifies the individual neuronal populations, and $Q_a^{\max}$ is the maximum firing rate. Based on previous studies, we set $Q_a^{\max}$ within the range of physiological parameters: $Q_e^{\max} = Q_i^{\max} = Q_r^{\max} = Q_s^{\max} = 250$ Hz, $Q_p^{\max} = 300$ Hz, $Q_d^{\max} = 65$ Hz, and $Q_\zeta^{\max} = 500$ Hz. The function $S$ is characterized by a gradual increase from 0 to $Q_a^{\max}$ as $V_a$ spans the entire real axis from negative to positive infinity. $\theta_a$ is the mean firing threshold, and $\sigma$ denotes the standard deviation of the corresponding threshold.

The membrane potential $V_a$ is determined by the incoming postsynaptic potentials from other neuronal populations and can be modeled as follows:

$$D_{\alpha\beta}V_a(t) = \sum_{b\in A} v_{ab}\phi_b(t). \tag{2.2}$$

Here, $D_{\alpha\beta}$ is a differential operator of the following form:

$$D_{\alpha\beta} = \frac{1}{\alpha\beta}\left[\frac{\partial^2}{\partial t^2} + (\alpha+\beta)\frac{\partial}{\partial t} + \alpha\beta\right], \tag{2.3}$$

which represents the dendritic filtering of the input signal. $\phi_b(t)$ is the field generated by the neuronal population $b$, which represents the input firing rate acting on other neuronal populations. Additionally, $\phi_n = 2mV_s$ is the nonspecific input to the SRN. $v_{xy}$ is the coupling strength from the neuronal population $y$ to $x$. $\alpha = 50\,s^{-1}$ and $\beta = 200\,s^{-1}$ correspond to the decay and rise times of the response to the input signal, respectively [9, 17].

In the input firing rate of the SRN, the delay parameter $\tau$ is specifically considered (i.e., $\phi_s(t-\tau)$), to account for the slow synaptic dynamics caused by the $GABA_B$ receptor-mediated second messenger process. According to previous studies, $\tau$ is set within the range of [20, 70] milliseconds. Throughout the network, each neuronal population generates a pulse field (axonal field) $\phi_a$, which propagates to other neuronal populations at an average conduction velocity $v_a$, and can be expressed as follows:

$$\frac{1}{\gamma_a^2}\left[\frac{\partial^2}{\partial t^2} + 2\gamma_a\frac{\partial}{\partial t} + \gamma_a^2 - v_a^2\nabla^2\right]\phi_a(t) = Q_a(t) \equiv S\left[V_a(t)\right]. \tag{2.4}$$

Given that the dynamical activity of absence seizures spreads throughout the brain, we assume that a homogeneous distribution in this mean-field model allows us to neglect its spatial derivatives (i.e., setting $\nabla^2 = 0$), which leads to the followings:

$$\frac{1}{\gamma_a^2}\left[\frac{\partial^2}{\partial t^2} + 2\gamma_a\frac{\partial}{\partial t} + \gamma_a^2\right]\phi_a(t) = Q_a(t). \tag{2.5}$$

Furthermore, compared to other neuronal populations, the axons of cortical excitatory pyramidal neurons ($e$) are sufficiently long. When $\phi_e$ propagates to other neuronal populations, it can generate significant projection effects, which can be modeled as follows:

$$\frac{d\dot{\phi}_e(t)}{dt} = \gamma_e^2\left[-\phi_e(t) + S\left(V_e(t)\right)\right] - 2\gamma_e\dot{\phi}_e(t), \tag{2.6}$$

where $\gamma_e = 100\,\mathrm{Hz}$ is the temporal damping rate that controls cortical impulses. The axons of the other nuclei are relatively short, and their propagation effects can be neglected. This can be expressed as follows:

$$\phi_j(t) = Q_j(t) \equiv S\left[V_j(t)\right] = \frac{Q_j^{\max}}{1 + \exp\left[-\frac{\pi}{\sqrt{3}}\frac{V_j(t)-\theta_j}{\sigma}\right]}, \quad j \in A,\ j \neq e. \tag{2.7}$$

Finally, considering that the strength of the cortical connections scales with the number of synapses engaged, we assume $V_e = V_i$ and $Q_e = Q_i$ [9, 11]. Therefore, incorporating the aforementioned modeling process, the first-order delayed differential equations of our improved BGCT model are given by the following:

$$\frac{d\phi_e(t)}{dt} = \dot{\phi}_e(t), \tag{2.8}$$

$$\frac{d\dot{\phi}_e(t)}{dt} = \gamma_e^2\left[-\phi_e(t) + F(V_e(t))\right] - 2\gamma_e\dot{\phi}_e(t), \tag{2.9}$$

$$\frac{dV_e(t)}{dt} = \dot{V}_e(t), \tag{2.10}$$

$$\frac{d\dot{V}_e(t)}{dt} = \alpha\beta\left(v_{ee}\phi_e - v_{ei}F(V_e) + v_{es}F(V_s) - v_{ed}F(V_d) - v_{ep}F(V_p) - V_e(t)\right) - (\alpha+\beta)\dot{V}_e(t), \tag{2.11}$$

$$\frac{dV_d(t)}{dt} = \dot{V}_d(t), \tag{2.12}$$

$$\frac{d\dot{V}_d(t)}{dt} = \alpha\beta\left(v_{de}\phi_e - v_{dd}F(V_d) + v_{ds}F(V_s) + v_{d\zeta}F(V_\zeta) - V_d(t)\right) - (\alpha+\beta)\dot{V}_d(t), \tag{2.13}$$

$$\frac{dV_p(t)}{dt} = \dot{V}_p(t), \tag{2.14}$$

$$\frac{d\dot{V}_p(t)}{dt} = \alpha\beta\left(-v_{pd}F(V_d) + v_{p\zeta}F(V_\zeta) - V_p(t)\right) - (\alpha+\beta)\dot{V}_p(t), \tag{2.15}$$

$$\frac{dV_\zeta(t)}{dt} = \dot{V}_\zeta(t), \tag{2.16}$$

$$\frac{d\dot{V}_\zeta(t)}{dt} = \alpha\beta\left(v_{\zeta e}\phi_e - v_{\zeta p}F(V_p) - V_\zeta(t)\right) - (\alpha+\beta)\dot{V}_\zeta(t), \tag{2.17}$$

$$\frac{dV_s(t)}{dt} = \dot{V}_s(t), \tag{2.18}$$

$$\frac{d\dot{V}_s(t)}{dt} = \alpha\beta\left(v_{se}\phi_e + v_{sr}F(V_r(t-\tau)) - V_s(t) + \phi_n\right) - (\alpha+\beta)\dot{V}_s(t), \tag{2.19}$$

$$\frac{dV_r(t)}{dt} = \dot{V}_r(t), \tag{2.20}$$

$$\frac{d\dot{V}_r(t)}{dt} = \alpha\beta\left(v_{re}\phi_e - v_{rp}F(V_p) + v_{rs}F(V_s) - V_r(t)\right) - (\alpha+\beta)\dot{V}_r(t). \tag{2.21}$$

The model adopts parameter settings aligned with empirical physiological data, as established in earlier research [9, 13]. Except where noted, numerical simulations employ the standard parameter settings listed in Table 1. Some parameters relate to the basal ganglia are modestly adjusted, while still staying within their usual biological ranges, so that the model reliably generates SWDs of 2 to 4 Hz under designated circumstances. Furthermore, we systematically adjust several key parameters (i.e., $-v_{sr}$ and $v_{ed}$) within a defined range to investigate different dynamic states and their potential impact on absence seizures.

The coupling strength for the direct connection between the STN and D neurons has not been quantified due to limited data and therefore needs to be approximated. Since the STN also sends GABAergic projections to the GPe, it can be logically concluded that the coupling strengths of these distinct STN projections are of similar magnitudes [38, 39]. Therefore, we consider it biologically reasonable to set the strength of the direct excitatory projection from the STN within 0–0.45 mV s.

### 2.3. Simulation method and data analysis

In this study, we employ a standard fourth-order Runge-Kutta integration scheme to perform numerical simulations in the MATLAB environment [9]. A diverse set of data analysis strategies is utilized to quantitatively assess the dynamic evolution and characteristics of SWDs in the model. All simulations are conducted with a fixed time resolution of 0.05 ms. Steady-state data within the time window of 5s to 25s are selected for the statistical analysis. To determine transition thresholds among various dynamical states, we conduct state and frequency analyses on the key model parameters. Specifically, for a given critical parameter, we analyze the system state change by plotting the local extremes (i.e., minima and maxima) of the steady-state cortical excitatory axon field as the parameter varied. This process requires all simulations to run for a sufficiently long duration (ensuring system stabilization before simulating an additional 10 seconds), and only time-series data from the stable phase are used to extract the local extrema. Through this analysis, we can clearly distinguish different dynamic states across parameter combinations. Furthermore, this technique facilitates the identification of dynamic state distributions within a two-parameter space.

We employ a power spectral analysis to estimate the core frequency of neural oscillations. The power spectral density is obtained by applying a Fast Fourier Transform (FFT) to a 10-second time series, and the dominant frequency of neural oscillations is defined as the frequency corresponding to the highest peak in the spectrum. By integrating the results of the state and frequency analyses, we precisely map the region in the two-parameter space where SWDs oscillations occur within the 2–4 Hz band. Additionally, to gain a more comprehensive understanding of the neural activity, we calculate the meaning firing rate (MFR) of key neural populations under specific conditions. In the numerical simulation, we select data from 5 to 25 seconds for the statistical analysis to ensure the stability of the results. To enhance the reliability, we conduct 20 independent simulations for each experimental condition, each with a different random seed, and the final reported results represent the averaged outcomes of these simulations.

**Table 1.** Model parameters.

| **Average Discharge Threshold** | **Population** | **Value (mV)** | **Source** |
|---|---|---|---|
| $\theta_e, \theta_i$ | EPN, IIN | 15 | [9, 11, 13, 19] |
| $\theta_s$ | SRN | 15 | [9, 11, 13, 19] |
| $\theta_r$ | TRN | 15 | [9, 12, 17, 19] |
| $\theta_\zeta$ | STN | 10 | [9, 12, 14, 19] |
| $\theta_d$ | D | 19 | [9, 14, 19] |
| $\theta_p$ | GPe | 9 | [9, 12, 19] |
| **Maximum Discharge Rate** | **Population** | **Value (Hz)** | **Source** |
| $Q_p^{max}$ | GPe | 300 | [9, 11, 17] |
| $Q_\zeta^{max}$ | STN | 500 | [9, 11, 17] |
| $Q_s^{max}$ | SRN | 250 | [9, 11, 17] |
| $Q_r^{max}$ | TRN | 250 | [9, 11, 17] |
| $Q_d^{max}$ | D | 65 | [9, 11, 17] |
| $Q_e^{max}, Q_i^{max}$ | EPN, IIN | 250 | [9, 11, 17] |

*Continued on next page*

| Coupling Weight | Pathway | Value (mV s) | Source |
|---|---|---|---|
| $v_{ee}$ | EPN → EPN | 1.0 | [9, 17] |
| $-v_{ei}$ | IIN → EPN | 1.8 | [9, 17] |
| $-v_{ed}$ | D → EPN | 0.45 (0–1) | [19] |
| $v_{es}$ | SRN → EPN | 1.801 | [9, 11, 17] |
| $-v_{ep}$ | GPe → EPN | 0.05 | [17] |
| $v_{de}$ | EPN → D | 1.01 | [9, 11, 17] |
| $-v_{dd}$ | D → D | 0.20 | [9, 17, 19] |
| $v_{ds}$ | SRN → D | 0.10 | [9, 11, 17] |
| $v_{d\zeta}$ | STN → D | 0.10 | Estimated |
| $-v_{pd}$ | D → GPe | 0.301 | [9, 17] |
| $v_{p\zeta}$ | STN → GPe | 0.45 | [9, 17, 38, 39] |
| $-v_{\zeta p}$ | GPe → STN | 0.04 | [9, 17] |
| $v_{\zeta e}$ | EPN → STN | 0.1004 | [9, 17] |
| $v_{se}$ | EPN → SRN | 2.20 | [9, 17] |
| $-v_{sr}$ | TRN → SRN | 0.80 | [9, 11, 17] |
| $-v_{rp}$ | GPe → TRN | 0.035 | [9, 11, 17] |
| $v_{rs}$ | SRN → TRN | 0.5001 | [9, 17] |
| $v_{re}$ | EPN → TRN | 0.05 | [10, 12, 19] |
| **Other Parameters** | **Meaning** | **Value** | **Source** |
| $\phi_n$ (mV s) | Sensory input to SRN | 2 | [9, 17] |
| $\sigma$ (mV) | Std. dev. of $\theta$ | 6 | [9, 17] |
| $\alpha$ ($s^{-1}$) | Rise time | 200 | [9, 17] |
| $\beta$ ($s^{-1}$) | Fall time | 50 | [9, 17] |
| $\gamma_e$ (Hz) | Damping rate of EPN | 100 | [9, 17] |
| $\tau$ (ms) | Time delay | 50 | [9, 17] |
| $\tau_1$ (ms) | Pulse delay | 4 | [34] |
| $\tau_2$ (ms) | Pulse delay | 2 | [34] |
| $\tau_3$ (ms) | Pulse delay | 2 | [34] |
| $\tau_4$ (ms) | Pulse delay | 3 | [34] |
| $A$ (mV) | Stimulus amplitude | 0-20 | Estimated |
| $f$ (Hz) | Stimulus frequency | 0-100 | Estimated |
| $W$ (ms) | Pulse width | 0-2 | Estimated |
| $v_{stim}$ (mV s) | Stimulus intensity | 0.785 | Estimated |

**Table 2.** List of abbreviations.

| Abbreviation | Full Form | Abbreviation | Full Form |
|---|---|---|---|
| BG | Basal Ganglia | STN | Subthalamic Nucleus |
| BGCT | Basal Ganglia-Corticothalamo | D | Striatum |
| SWDs | Spike-Wave Discharges | FPS | Four-phase Pulse Stimulation |
| EPN | Cortical Excitatory Neurons | IIN | Inhibitory Interneurons |
| SRN | Specific Relay Nucleus | TRN | Thalamic Reticular Nucleus |
| GPe | External Globus Pallidus | SNr | Substantia Nigra pars reticulata |
| MFR | Meaning Firing Rates | LFS | Low firing State |
| OS | Simple Oscillatory State | SFS | Saturation Firing State |

## 3. Results

### *3.1. The improved model can reproduce four dynamic states*

Previous studies showed that the slow dynamics of $GABA_B$ receptors in the TRN are a potential pathological factor which contributes to absence seizures in both animal experiments and biophysical models of the cortico-thalamic network [40, 41]. In order to determine if this abnormal mechanism leads to 2–4 Hz SWDs in the model, we analyze the effects of two main parameters: the inhibitory projection strength ($-v_{sr}$) and its corresponding time delay ($\tau$). Then, we conduct state and frequency analyses in a two-dimensional parameter space (Figures 2(a),(b)).

Consistent with previous findings [9, 17], four distinct dynamic states emerge in the system (Figure 2(a)): (I) Low Firing State (LFS), characterized by stable network activity without oscillations (0 Hz), which corresponds to a normal neuronal resting state; (II) Simple Oscillations State (OS), which exhibits a single oscillation peak per cycle and represents physiological rhythmic activity; (III) SWDs State, which captures the 2–4 Hz oscillations with two peaks per cycle typical of absence seizures; and (IV) Saturation Firing State (SFS), a non-physiological condition where the firing rate approaches 250 Hz without an oscillatory behavior. In cases where $-v_{sr}$ exhibits a low coupling strength, the inhibitory effect of the TRN fails to effectively suppress the SRN firing. Due to a strong excitatory drive from pyramidal neurons, the SRN rapidly becomes highly active once the simulation begins, which subsequently causes the cortical neurons to reach a firing saturation (IV, Figure 2(a)) within a brief oscillatory period. As $-v_{sr}$ increases, the inhibitory effect of the TRN begins to modulate SRN firing (Figures 2(c),(d)). For a sufficiently large $\tau$, our model sequentially undergoes the SWDs oscillations (III, Figure 2(a)) and the OS (II, Figure 2(a)). However, if $-v_{sr}$ is too strong, then the TRN almost completely suppresses the oscillatory activity. In this case, the system transitions into the LFS (I, Figure 2(a)). Furthermore, we observe that the delay associated with $GABA_B$ transmission has a pronounced effect on the system's dynamic behavior. In particular, the emergence of SWDs within the model requires a sufficiently large value of $\tau$ (Figure 2(a)).

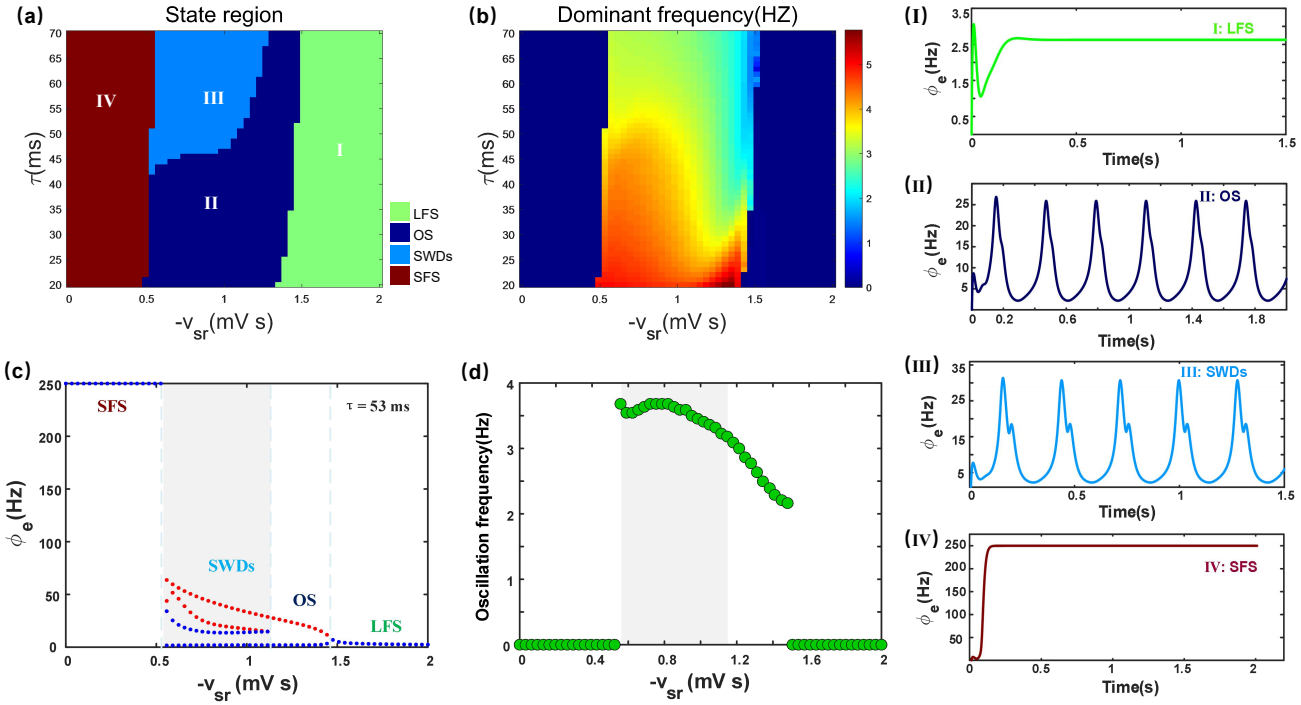


**Figure 2.** Analysis of dynamical states (a) and frequency (b) responses in the two-dimensional parameter space $(-v_{sr}, \tau)$. Different states are represented by different colors in (a), while (b) shows the corresponding frequency range. (I) low firing, (II) simple oscillations, (III) SWDs, (IV) saturation. In particular, the parameters corresponding to the time series of the four states in the lower panels are chosen as follows: (I) $-v_{sr} = 1.75$ mV s, $\tau = 50$ ms; (II) $-v_{sr} = 1$ mV s, $\tau = 30$ ms; (III) $-v_{sr} = 1$ mV s, $\tau = 50$ ms; and (IV) $-v_{sr} = 0.25$ mV s, $\tau = 50$ ms. Analysis of dynamical states (c) and frequency (d) in the one-dimensional parameter $-v_{sr}$. In all simulations, we set $v_{d\zeta} = 0.1$ mV s.

### *3.2. The impact of the newly identified STN-D pathway on SWDs*

Recent experimental data suggest the existence of a direct projection from the STN to the D [22]. Theoretically, the excitatory output of this pathway can shape the firing activity of striatal neurons, which, in turn, exerts an inhibitory effect on the cortex. This may provide a potential mechanism to regulate absence seizures. We test this hypothesis by examining the role of the excitatory coupling strength $v_{d\zeta}$ in the STN-D pathway, which is involved in controlling absence seizures. In the next subsection, we keep $v_{d\zeta}$ constant and introduce an external excitatory stimulus, $V_{\mathrm{SD}}$, to the D. This method allows for the precise modulation of striatal neuronal firing rates and enables the examination of whether their activation levels contribute to seizure regulation.

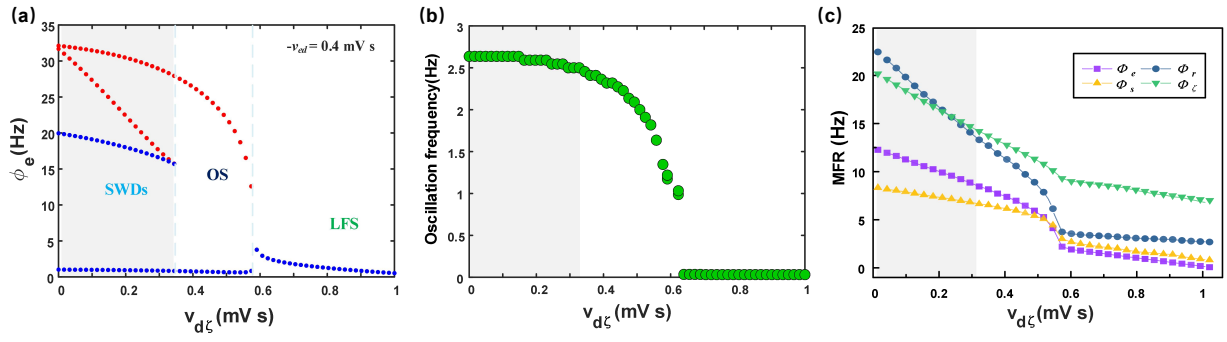


**Figure 3.** Suppression of SWDs via direct excitatory STN-D projections. (a) State analysis of the one-dimensional parameter $v_{d\zeta}$, where $v_{d\zeta}$ represents the strength of excitatory coupling of the STN-D projection. (b) The oscillatory frequency (OF) of the EPN as a function of $v_{d\zeta}$. (c) The MFR of key nuclei as $v_{d\zeta}$ increases.

Figure 3(a) is an extremum plot, which illustrates the changes in the system's dynamical states under different values of $v_{d\zeta}$. With the increase of $v_{d\zeta}$, three dynamical states of the system appear as it follows the SWDs, OS, and LFS. Figure 3(b) shows a graph of the oscillation frequency (OF) of the EPN, from which we can see that the frequency of the SWDs is usually in the range of 2–4 Hz. Figure 3(c) presents the variation of the MFR of different neural nuclei as a function of $v_{d\zeta}$, thus highlighting key characteristics of the system's dynamic state. Overall, as $v_{d\zeta}$ increases, the system state transitions from SWDs to OS, and the MFR of each neural nucleus shows a decreasing trend, which indicates that $v_{d\zeta}$ has an inhibitory effect on the neural activity. Notably, around $v_{d\zeta} \approx 0.58$ mV s, a significant transition in the MFR of certain neural nuclei is observed, thus suggesting a possible dynamical bifurcation or state transition in the system. The gray-shaded region corresponds to the critical transition zone where the system shifts from SWDs (pathological state) to LFS (stable state), further highlighting the sensitivity of this parameter in regulating the system dynamics. Different neural nuclei exhibit varying responses to changes in $v_{d\zeta}$. For instance, $\phi_e$ and $\phi_\zeta$ have higher firing rates and steeper slopes as $v_{d\zeta}$ varies, thus indicating a greater sensitivity to this parameter. In contrast, $\phi_r$ exhibits a consistently lower firing rate and changes more gradually, thus indicating a possible auxiliary role in the system regulation.

The combination of Figures 3(a),(c), reveal the characteristics of the dynamical behavior as $v_{d\zeta}$ increases. When $v_{d\zeta}$ is within the lower range (0 – 0.3 mV s), the system exhibits a stable SWDs state, with relatively low and steady frequency and firing rates. As $v_{d\zeta}$ approaches a critical value (about 0.35 mV s), the system transitions abruptly from the SWDs state to the OS, which is characterized by a rapid increase in frequency and a significant rise in the firing rate. Further increasing $v_{d\zeta}$ (> 0.6 mV s) shifts the system into the LFS, where both the frequency and firing rates decrease to lower levels. The extremum plot provides a global perspective on the system's macrodynamics, while the mean firing rate plot quantifies the activity levels of neural nuclei at a microscopic level. The combination of these two analyses effectively characterizes the system's state evolution.

### 3.3. *The effect of striatal activation level on SWDs modulation*

To further understand the mechanism by which the activation level of the D regulates SWDs, we apply an external positive stimulation voltage ($V_{SD}$) to the D to investigate the effect on controlling SWDs. Theoretically, an increase in $V_{SD}$ can directly increase the activation level of the D, which, in turn, can directly exert an inhibitory effect on the cortex. As shown in Figure 4(a), with the increase of $V_{SD}$, two states appear in the system, namely SWDs and OS. The frequency of the SWDs is in the range of 2–4 Hz, as shown in Figure 4(b). Consistent with the theoretical results, we find that an increase in the D activation level can cause the system to transition from the SWDs to LFS. To gain a more comprehensive understanding of neural activity, we also simulate the MFR of the D (Figure 4(c)). As expected, the MFR of the D essentially increase with the increase of $V_{SD}$, which is attributed to the fact that $V_{SD}$ can directly increase the D activation and thus the inhibitory effect of the EPN. This strengthened inhibitory influence reduces the overall excitatory drive within the cortical network, thereby decreasing the MFR of the EPN. Thus, SWDs are effectively suppressed due to the diminished excitability of the cortical-thalamic circuitry.

The above findings suggest that enhancing the D activation can efficiently inhibit SWDs. We further propose that the four direct inputs to the D may modulate its activity and contribute to the SWD regulation.

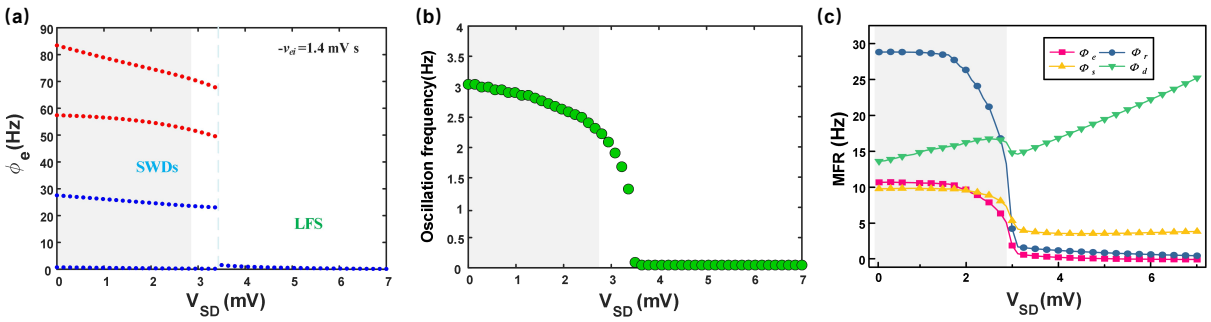


**Figure 4.** Inhibited SWDs induced by the activation level ($V_{SD}$) of the D. One-dimensional state analysis (a) and frequency analysis (b) along the parameter $V_{SD}$. As the $V_{SD}$ increases, the system state gradually transitions from SWDs to LFS. (c) The variation of the MFR of key neural nuclei as a function of $V_{SD}$. Here, we set $v_{d\zeta} = 0.1$ mV s.

#### 3.3.1. The effect of direct striatal input on SWDs modulation

In this study, we explore how direct afferent inputs to the D influence SWDs regulation. As illustrated in Figure 1, the D receives excitatory projections from the STN, EPN, and SRN, along with inhibitory self-connections. These afferent pathways influence the firing behavior of the D and may be critical to modulate SWDs. In the previous section, we discuss the effect of the newly incorporated direct STN-D projection in modulating SWDs. In this section, we further examine the participation of three other direct striatal input pathways: SRN-D, EPN-D, and D-D to determine whether and how they contribute to the modulation of SWDs. Moreover, the analysis of the regulatory roles of these four

direct pathways lays the foundation to subsequently apply functionally substitutive stimulations to the D nucleus.

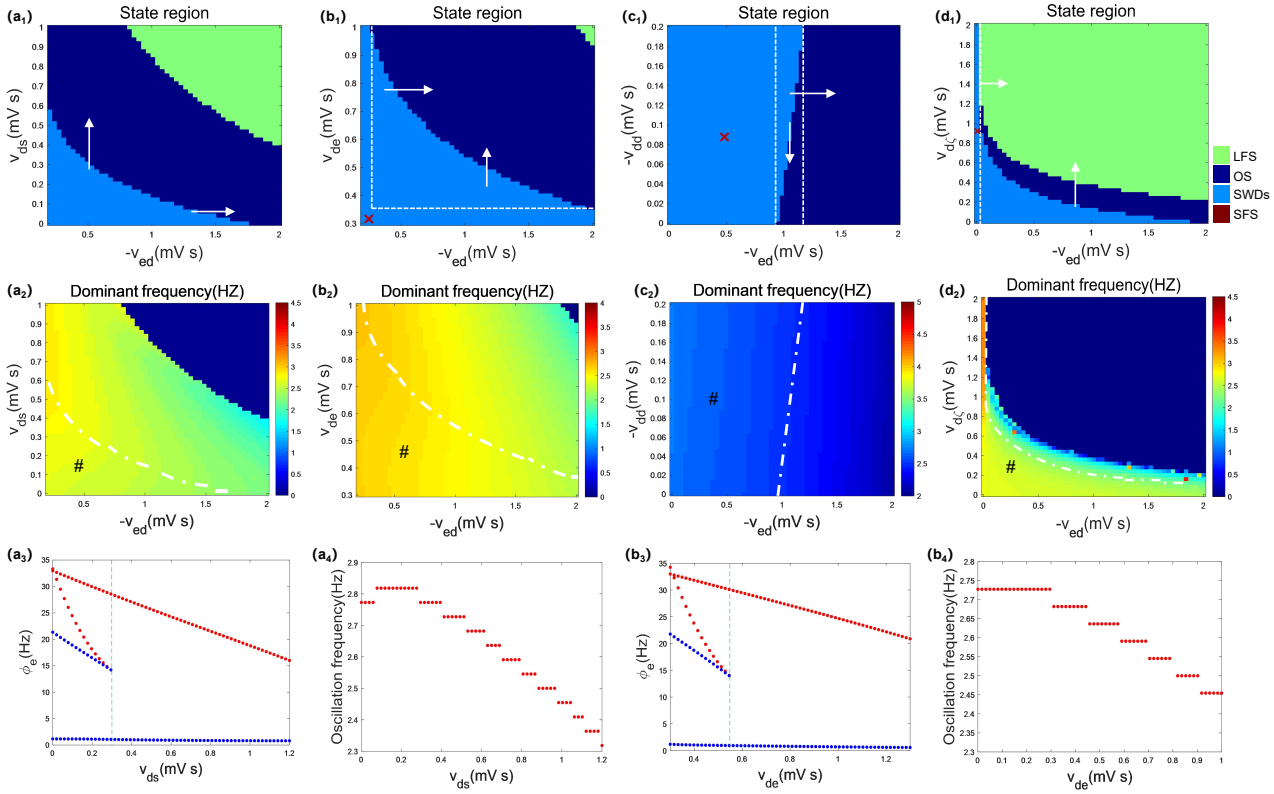


**Figure 5.** The effect of direct D input pathways on SWDs modulation. ($a_1$), ($b_1$), ($c_1$), and ($d_1$) are the state analyses of the two-dimensional parameter spaces ($-v_{ed}$, $v_{ds}$), ($-v_{ed}$, $v_{de}$), ($-v_{ed}$, $-v_{dd}$), and ($-v_{ed}$, $v_{d\zeta}$), respectively. ($a_2$), ($b_2$), ($c_2$), and ($d_2$) are the corresponding frequency analyses. ($a_3$) and ($a_4$) are the one-dimensional parametric extreme diagram and main frequency diagram as a function of the $v_{ds}$, respectively; ($b_3$) and ($b_4$) are the one-dimensional parametric extreme diagram and main frequency diagram as a function of the $v_{de}$, respectively. Here, $v_{ds}$ denotes the coupling strength of the excitatory STN-D pathway, $v_{de}$ refers to the coupling strength of the excitatory EPN-D pathway, $-v_{dd}$ represents the coupling strength of the inhibitory D-D pathway, and $v_{d\zeta}$ refers to the coupling strength of the excitatory STN-D pathway. The direction of the arrow indicates the direction of suppressing the SWDs. In ($a_2$), ($b_2$), ($c_2$), and ($d_2$), the "#" region surrounded by the white dashed line corresponds to the typical 2–4 Hz SWDs parameter range. The red symbol "×" indicates that SWDs cannot be adjusted in this area.

We select the coupling strength of the D to the cortex pathway ($-v_{ed}$) as the horizontal axis variable, primarily because this pathway directly regulates the cortical activity in the model. The direct inhibitory projection from the D to the cortex represents a key regulatory mechanism, and changes in its coupling strength can significantly affect the cortical excitability, thereby altering the

overall dynamical state of the system. To explore how different direct input pathways influence the regulation of SWDs, we examine the system state and dominant frequency distributions in four two-parameter spaces: $(-v_{ed}, v_{ds})$, $(-v_{ed}, v_{de})$, $(-v_{ed}, -v_{dd})$, and $(-v_{ed}, v_{d\zeta})$, as shown in Figures 5($a_1$)–5($d_2$), respectively. Three major activity regimes (SWDs, OS, and LFS) are identified in most panels, while only SWDs and OS appear in the $(-v_{ed}, -v_{dd})$ space. Arrows indicate directions in which the system transitions away from SWDs. These results demonstrate that all four input pathways contribute to the modulation of SWDs. Excitatory projections from the EPN, STN, and SRN tend to enhance the D neuron activity as their coupling strengths increase, whereas a stronger inhibitory D-D self-connection reduces the striatal activation. A higher activation level of the D implies a stronger inhibition of the EPN, thus potentially leading to SWD suppression. Consistent with our findings, strengthening $v_{ds}$, $v_{d\zeta}$, and $v_{de}$ facilitates the transition from SWDs to OS, thus demonstrating effective suppression (Figures 5($a_1$),($b_1$),($d_1$)). In contrast, the self-feedback coupling strength $-v_{dd}$ has a relatively minor impact on the system states, which can only be regulated in a small range, as indicated by the arrows in Figure 5($c_1$). The effectiveness of these parameters in controlling SWDs depends on the coupling strength of the D-EPN projection. When $-v_{ed}$ is sufficiently strong, the D's output significantly inhibits the EPN. Under this condition, for default values of $v_{ds}$, $v_{de}$, $-v_{dd}$, and $v_{d\zeta}$, the system remains in either the OS or the LFS.

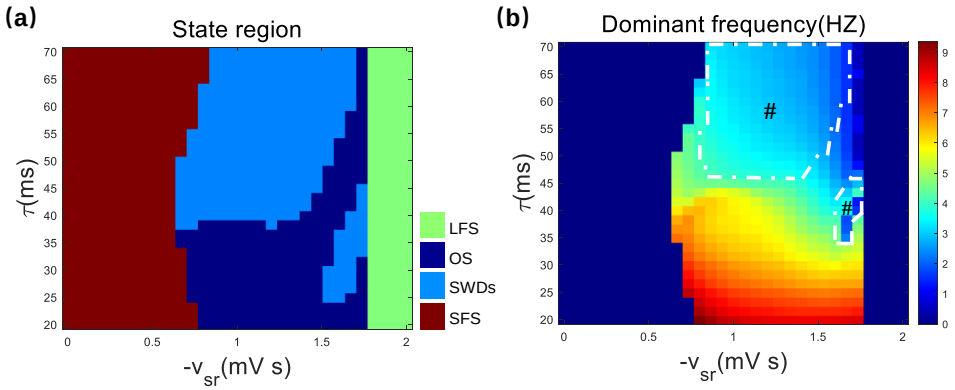


**Figure 6.** (a) Analysis of dynamic states within a two-dimensional domain of parameters $(-v_{sr}, \tau)$ under the condition that there is no SRN, EPN, STN, and D input to the D ($v_{ds} = v_{d\zeta} = v_{dd} = v_{de} = 0$); (b) Two-dimensional frequency analysis of the panel corresponding to the conditions in (a) $(-v_{sr}, \tau)$, where $-v_{sr}$ represents the connection strength from the TRN to SRN, and $\tau$ is the time delay of $GABA_B$ connections. The "#" region enclosed by the white dashed line corresponds to the typical 2–4 Hz SWDs parameter range.

Next, we further investigate the multiple regulatory effects of the four pathways: STN-D, SRN-D, EPN-D, and D-D. As shown in Figure 6, panels (a) and (b) illustrate the two-parameter state diagram of $(-v_{sr}, \tau)$ and the corresponding primary frequency evolution in the absence of the SRN, EPN, STN, and D inputs to D (i.e., $v_{ds} = v_{d\zeta} = v_{dd} = v_{de} = 0$). Compared to Figure 2(a), Figure 6(a), which

represents the case without inputs to the striatum (D), shows a rightward shift of the onset pattern in the $(-v_{sr}, \tau)$ parameter plane. The SFS region expands, the LFS region shrinks, and the SWDs region significantly increases. Specifically, the proportion of the SWDs state increases from 12.71% in Figure 2(a) to 29.24% in Figure 6(a). These results suggest that the STN-D, SRN-D, EPN-D, and D-D pathways play a regulatory role in seizure dynamics via their influence on the striatal activity.

### 3.3.2. Independent effects of individual D-input pathways on SWDs

To investigate the independent effects of each pathway, we block the four inputs to the D one at a time and observe how the remaining pathways influence the seizure patterns. In Figure 7, we block (by setting the coupling strength to zero) the EPN-D (Figure 7($a_1$)), STN-D (Figure 7($b_1$)), SRN-D (Figure 7($c_1$)), and D-D (Figure 7($d_1$)) pathways. We can analyze the independent effects of each pathway by comparing Figure 7 with Figure 2 without blocking the EPN-D, STN-D, SRN-D, or D-D pathways.

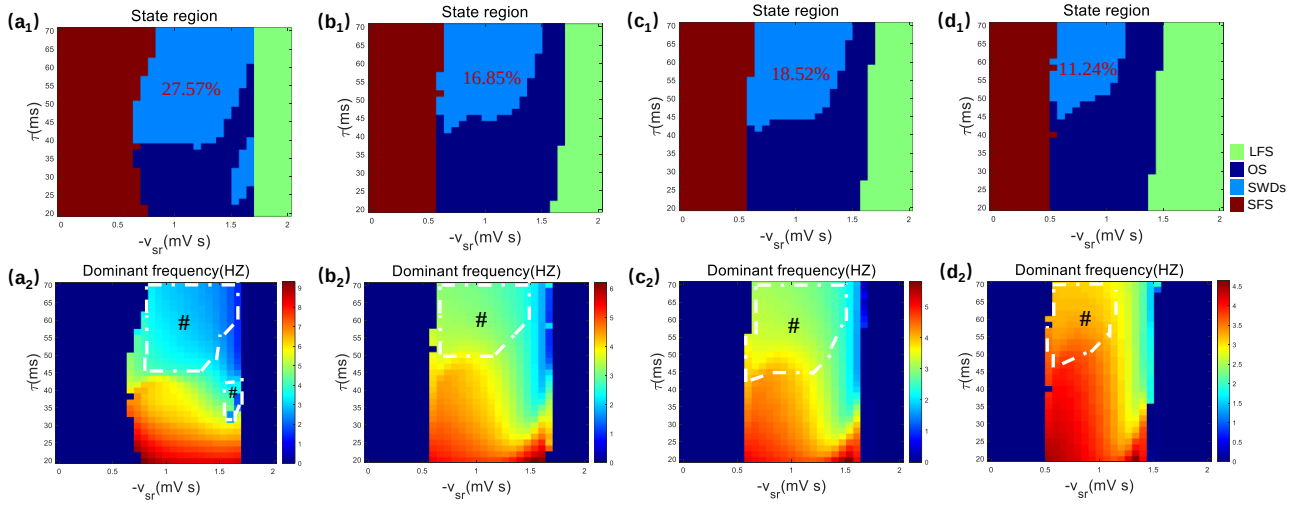


**Figure 7.** State and frequency diagrams as the effects of selectively blocking each of the four direct input pathways to the D nucleus on seizure dynamics. ($a_1$) State analysis on the two-dimensional plane of $(-v_{sr}, \tau)$ in the absence of EPN input ($v_{ds}$ = 0.1 mV s; $v_{d\zeta}$ = 0.1 mV s; $v_{dd}$ = 0.2 mV s; $v_{de}$ = 0 mV s); ($b_1$) Analysis of dynamic states within a two-dimensional domain of parameters $(-v_{sr}, \tau)$ in the absence of STN input ($v_{ds}$ = 0.1mV s; $v_{d\zeta}$ = 0 mV s; $v_{dd}$ = 0.2 mV s; $v_{de}$ = 1 mV s); ($c_1$) Analysis of dynamic states within a two-dimensional domain of parameters $(-v_{sr}, \tau)$ in the absence of SRN input ($v_{ds}$ = 0 mV s; $v_{d\zeta}$ = 0.1 mV s; $v_{dd}$ = 0.2 mV s; $v_{de}$ = 1 mV s); ($d_1$) Analysis of dynamic states within a two-dimensional domain of parameters $(-v_{sr}, \tau)$ in the absence of D input ($v_{ds}$ = 0.1 mV s; $v_{d\zeta}$ = 0.1 mV s; $v_{dd}$ = 0mV s; $v_{de}$ = 1 mV s). ($a_2$), ($b_2$), ($c_2$), and ($d_2$) show the frequency analysis corresponding to ($a_1$), ($b_1$), ($c_1$), and ($d_1$), respectively. The "#" region surrounded by the white dashed line corresponds to the typical 2–4 Hz SWDs parameter range.

Compared to Figure 2(a), where the proportion of the SWDs state is 12.07%, blocking the EPN–D pathway, as shown in Figure 7($a_1$), results in a marked redistribution of state regions in the ($-v_{sr}$, $\tau$) parameter plane. Notably, the proportion of the SWDs state increases to 27.57%, which indicates that the EPN-D pathway plays a crucial role in modulating seizure dynamics through its regulation of the striatal activity. After blocking the STN-D pathway (Figure 7($b_1$)) and the SRN-D pathway (Figure 7($c_1$)), the state area shows moderate changes and the main frequency distribution is adjusted; however, the SWDs state area also increases compared with Figure 2(a). Although their effects are weaker than those of the EPN-D pathway, both pathways also play important roles in modulating specific states and frequency ranges. In contrast, the changes in the state area and the main frequency distribution due to blocking the D-D pathway (Figure 7($d_1$)) are not significant, and the proportion of the SWDs state decreases to 11.24%, which suggests that the self-suppression of the D has a minimal effect on the overall dynamic pattern. Consistent with this theory, the D-D self-inhibition suppresses the striatal activity. Blocking this pathway enhances striatal activation, thereby increasing its inhibitory effect on the cortex and reducing the extent of SWDs. When the other three excitatory pathways are blocked, they decrease striatal activation, which, in turn, has a diminished inhibitory effect on the cortex, thus leading to an increase in the extent of SWDs.

A comprehensive analysis reveals that the EPN-D pathway has the most significant effect on the seizure pattern regulation, followed by the STN-D and SRN-D pathways, whereas the D's self-inhibition has a relatively minor influence. These findings highlight the differential roles of each pathway in modulating seizure patterns, thus providing a foundation for the further exploration of their physiological mechanisms.

#### 3.3.3. Multiple effects of EPN-D, STN-D, D-D, and SRN-D pathways

We analyze the impact of adjusting the parameters $v_{de}$, $v_{d\zeta}$, $v_{ds}$, and $v_{dd}$ on the system state (Figure 8). The results indicate that as $v_{de}$ increases, the SWDs state gradually diminishes, and the system transitions to either a simple oscillatory state or a resting state, thus suggesting that increasing $v_{de}$ is an effective strategy for suppressing the SWDs. Furthermore, when $v_{de}$ is relatively small, increasing $v_{d\zeta}$ and $v_{ds}$ can also suppress the SWDs, which leads the system into a resting state. When $v_{de}$ is within a moderate range, reducing $v_{dd}$ helps diminish the SWDs state and facilitates a transition to the OS. A frequency analysis further demonstrates that the SWDs state is generally associated with a lower dominant frequency, whereas the OS corresponds to a higher dominant frequency. As $v_{de}$ increases, the low-frequency region gradually shrinks while the high-frequency region expands, thus confirming the effectiveness of $v_{de}$ modulation in suppressing SWDs.

In summary, appropriate adjustments of these parameters enable an effective transition from the SWDs to either the OS or the LFS, thus providing theoretical support for seizure control.

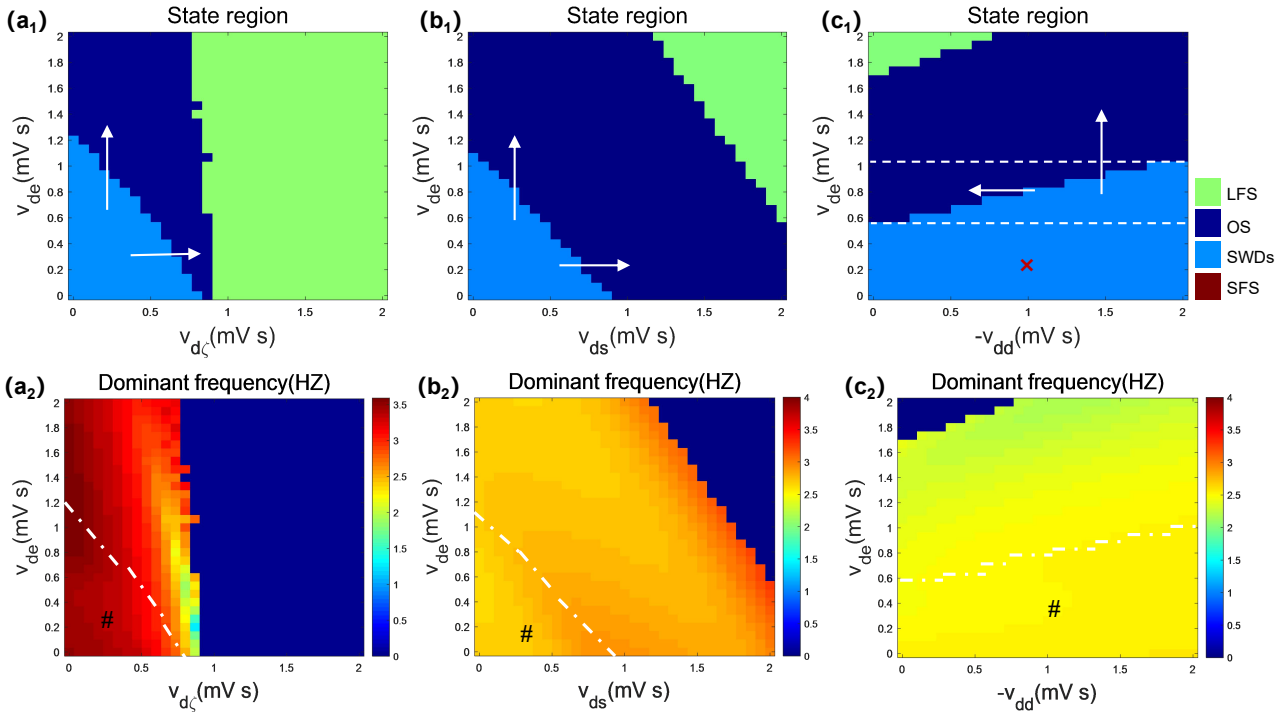


**Figure 8.** Multiple effects of EPN-D, STN-D, D-D, and SRN-D pathways for modulating SWDs. ($a_1$), ($b_1$), and ($c_1$) are state analyses on the two-dimensional parameter planes ($v_{d\zeta}$, $v_{de}$), ($v_{ds}$, $v_{de}$), and ($v_{dd}$, $v_{de}$), respectively; ($a_2$), ($b_2$), and ($c_2$) show the frequency analyses that correspond to ($a_1$), ($b_1$), and ($c_1$), respectively. The "#" region surrounded by the white dashed line corresponds to the typical 2–4 Hz SWDs parameter range. The arrows indicate the direction of SWDs suppression. The red symbol "×" indicates that the SWDs cannot be adjusted in this area. Here, we set $-v_{sr} = 1$ mV s, $\tau = 50$ ms.

## 4. Effects of a novel stimulation pattern on the striatum

Here, we remove the four inputs to the D to simulate the replacement effect of our newly discovered stimulation pattern on the striatal inputs. Without affecting the original internal control, we apply external stimulation to the D to investigate how such stimulation modulates absence seizures. We present the following equation of the model with external stimulation:

$$\frac{d\dot{V}_d(t)}{dt} = \alpha\beta\left(v_{stim}F(t_s)\right) - (\alpha+\beta)\dot{V}_d(t). \tag{4.1}$$

The external stimulation ($t_s$) is processed by the Sigmoid function $F$, applied to the D, and multiplied by the stimulation intensity parameter $v_{stim}$, which is the only input to the D.

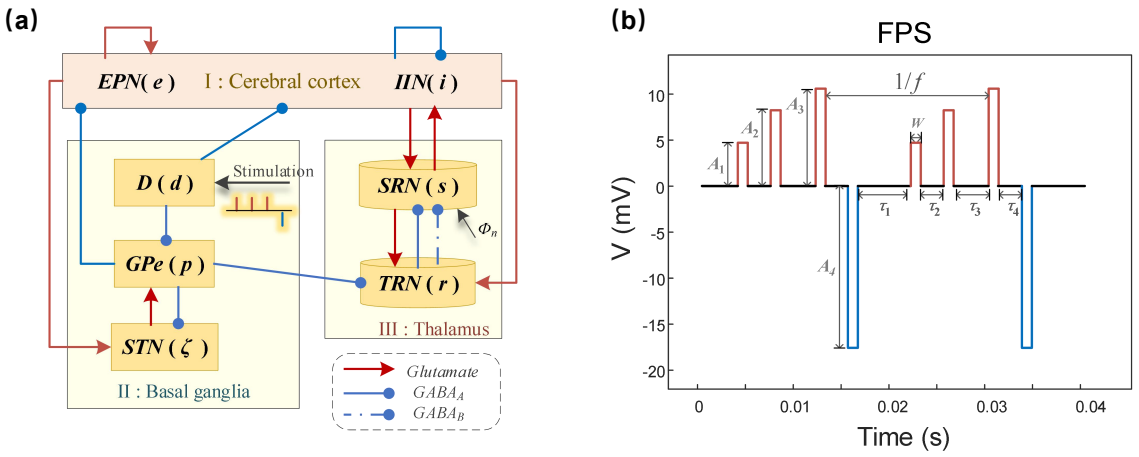


**Figure 9.** (a) Schematic diagram of the model structure with stimulation pulses replacing the original inputs to the D. Synaptic connections are represented by different lines (arrowed lines: glutamatergic excitatory connections; solid circular-headed lines: $GABA_A$ inhibitory connections; dashed circular-headed lines: $GABA_B$ inhibitory connections). (b) Schematic of the stimulation waveform with three anodal and one cathodal phase. The pulse delays are set as $\tau_1 = 4$ ms, $\tau_2 = 2$ ms, $\tau_3 = 3$ ms, and $\tau_4 = 3$ ms; $A_1$, $A_2$, $A_3$, and $A_4$ denote the pulse amplitudes. $W$ represents the pulse width, set at 1 ms, and $f$ denotes the stimulation frequency.

The novel stimulation pattern that we proposed (FPS, as shown in Figure 9) applies four-phase pulses sequentially to the D in each cycle, thus representing inputs from the EPN, SRN, STN, and D, respectively. We assume that the original four input pathways of the D are either damaged or interrupted, and the FPS is used to replace the regulatory functions of these damaged or missing pathways. The stimulation pattern incorporates time intervals, which better align with the rhythm of physiological stimulation. The transmission delay is referenced from observations of pathway delays in SNr neurons of the basal ganglia [34]. In each FPS cycle, the first three phases are positive (anodic phases), thus representing the excitatory effects of the SRN-D, STN-D, and EPN-D, respectively. The subsequent cathodic phase represents the self-inhibitory effect of the D-D. The stimulation amplitudes are denoted by $A_1$, $A_2$, $A_3$, and $A_4$. $W$ represents the pulse width, and $f$ denotes the stimulation frequency. In Hou et al.'s simulation, the settings of $A$, $f$, and $W$ were validated to effectively modulate the neuronal firing behavior and suppress absence seizures in the model [34]. Therefore, we make adaptive adjustments on this basis to ensure that the parameter ranges are suitable for this model. The FPS can be modeled as follows:

$$t_s = \begin{cases} A_1, & t \in (k\tau_1,\ k(\tau_1 + W)) \\ A_2, & t \in (k(\tau_1 + \tau_2 + W),\ k(\tau_1 + \tau_2 + 2W)) \\ A_3, & t \in (k(\tau_1 + \tau_2 + \tau_3 + 2W),\ k(\tau_1 + \tau_2 + \tau_3 + 3W)) \\ A_4, & t \in (k(\tau_1 + \tau_2 + \tau_3 + \tau_4 + 3W),\ k(\tau_1 + \tau_2 + \tau_3 + \tau_4 + 4W)) \\ 0, & \text{otherwise}, \end{cases} \tag{4.2}$$

where $k = 1, 2, 3, \ldots$, and $\tau_1$, $\tau_2$, $\tau_3$, $\tau_4$ represent the time delays. The input signal to the D is obtained through a weighted sigmoid function, which converts the time series of the stimulation into the rate of stimulation over time. $v_{stim}$ is the total stimulation intensity from the electrode, and we set $v_{stim} = 0.785$ mV s.

Traditional DBS stimulation patterns typically employ either single-frequency or simple frequency-modulated electrical pulse stimulation. In contrast, the FPS introduced in this study consists of three positive phases (excitatory inputs) and one negative phase (inhibitory input). Through the alternating interaction of different phases, the FPS better adapts to the dynamic characteristics of neural circuits, avoids side effects from excessive electrical stimulation, and enhances the therapeutic efficacy. This novel stimulation pattern aims to explore its potential to replace the striatal input, thus providing a theoretical foundation for the innovation of DBS technology.

### *4.1. Stimulation amplitude on the control effect of the four pathways*

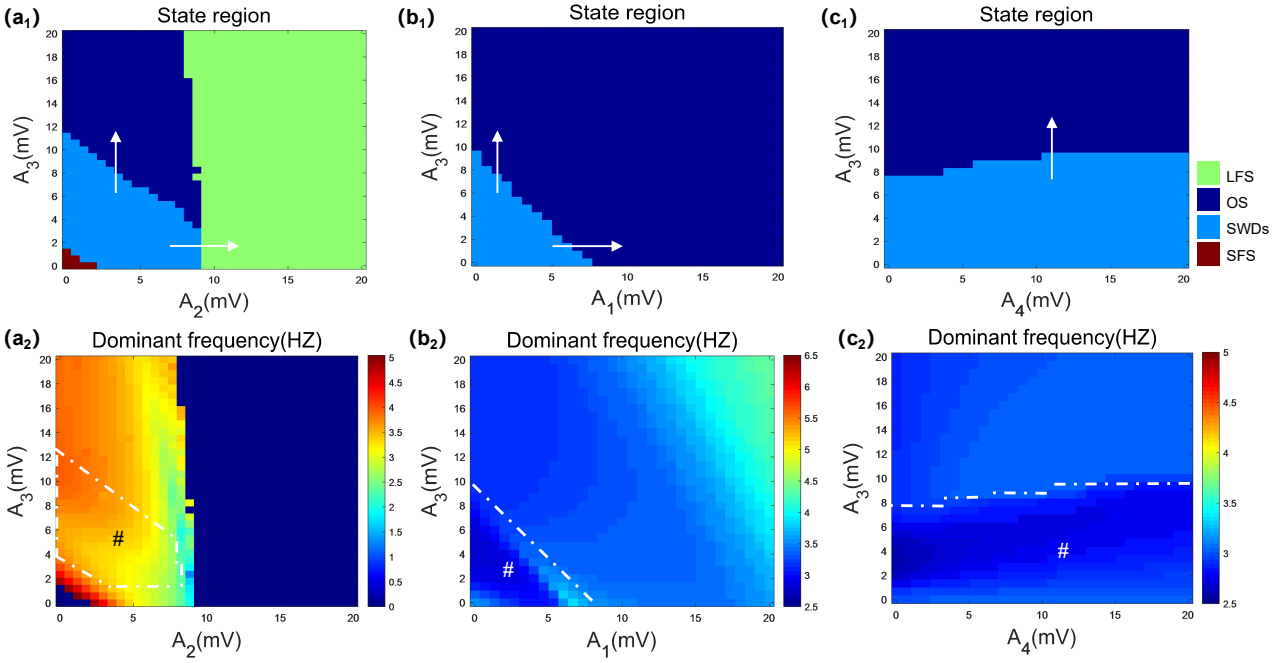


**Figure 10.** State and frequency diagrams illustrate the effects of the FPS as a functional substitute for the four direct striatal input pathways. ($a_1$) and ($a_2$) are the state analyses and the corresponding principal frequency analyses on the two-dimensional plane consisting of the phase amplitudes $A_2$ and $A_3$ of the FPS, respectively, with a fixed phase amplitude $A_1, A_4 = 10$ mV. ($b_1$) and ($b_2$) are state analyses and corresponding main frequency analyses on a two-dimensional plane consisting of phase amplitudes $A_1$ and $A_3$, respectively, with fixed phase amplitudes $A_2, A_4 = 10$ mV. ($c_1$) and ($c_2$) are the state analyses and the corresponding principal frequency analyses on a two-dimensional plane consisting of phase amplitudes $A_4$ and $A_3$, respectively, with phase amplitudes $A_1, A_2 = 10$ mV. Other parameters are set to their default values (Table 1), with a stimulation frequency of $f = 50$ Hz, $W = 1$ ms, and $v_{stim} = 0.785$ mV s.

We propose a novel stimulation paradigm in which four-phase pulses (anodal phases $A_1$, $A_2$, $A_3$, and $A_4$) are continuously applied to the D in each cycle, thus simulating the excitatory inputs from the SRN, STN, and EPN, as well as the self-inhibition of the D. The results show that increasing the amplitude of the anodal phase pulse $A_3$ (EPN-D input) effectively suppresses SWDs discharges, thus facilitating a transition to the OS. Increasing $A_1$ (SRN-D input) and $A_2$ (STN-D input) further promotes the transition from the SWDs to either the LFS or the OS. This indicates that the excitatory inputs from the SRN, STN, and EPN play a crucial role in seizure regulation.

Additionally, adjusting the amplitude of the cathodal phase pulse $A_4$ (D-D self-inhibition input) has a relatively minor effect on the system state, thus suggesting that striatal self-inhibition has a limited role in SWDs formation. Therefore, the cathodal pulse intensity can be set relatively high—on one hand, this has minimal impact on the system, and on the other, it ensures charge balance between positive and negative phases. Compared to conventional stimulation paradigms, alternating-electrode stimulation also causes less tissue damage.

By comparing these results with the direct parameter modulation in the system (Figure 8), we observe that the FPS paradigm successfully replaces the original striatal inputs and achieves an effective control over absence seizures by adjusting the anodal-phase inputs. Furthermore, the FPS exhibits superior seizure suppression when jointly modulating the amplitudes of the anodal-phase pulses $A_1$, $A_2$, and $A_3$), while reducing the reliance on striatal self-inhibition ($A_4$). This further confirms the key role of excitatory inputs from the SRN, STN, and EPN in SWDs formation and regulation.

In conclusion, the FPS paradigm provides a novel theoretical basis and potential technological support for the application of external neural stimulation in epilepsy control.

### *4.2. Combined effects of frequency and pulse width under synchronous amplitude modulation*

In addition to the amplitudes of each phase in the FPS, previous studies demonstrated that the stimulation frequency and pulse width also play crucial roles in modulating the control efficacy of external stimulation [42]. To simplify the analysis, we assume that the amplitudes of the four-phase components vary in unison. Based on this assumption, we separately explore how the combined influence of the stimulation amplitude interacts with the frequency ($f$) and the pulse width ($W$). Figures 11($a_1$),($b_1$) illustrate the distribution of states and the corresponding frequencies across the two-dimensional parameter plane defined by($f$, $A$), while Figures 11($a_2$) and ($b_2$) depict the same analyses over the ($W$, $A$) parameter domain. In Figure 11($a_1$), the two dashed lines represent the positions at frequencies of 40 Hz and 90 Hz, respectively; it can be observed that the SWDs region slightly decreased.

The results indicate that $A$ is the key parameter that influences the system state. When the stimulation amplitude is low, the system primarily remains in the SWDs state. As $A$ increases, the system gradually transitions from the SWDs to the OS and enters the LFS when $A > 10$ mV. The effect of the stimulation frequency on the system state is relatively weak. However, at higher frequencies, both the system state region and the dominant frequency change, which suggests that it may play an auxiliary role in the state transitions. Compared to $f$, the pulse width $W$ has a negligible effect on the system state; under both small and large pulse widths, the SWDs state remains virtually unchanged. A comprehensive analysis indicates that $A$ is the dominant factor in the system state transitions, and directly drives the system to transition from the SWDs to either the OS or the LFS. In contrast, $f$ and $W$ play auxiliary optimization roles. By adjusting the $f$ and $W$, a more efficient state control can

be achieved under low-amplitude stimulation. These findings provide valuable guidance for selecting optimal stimulation parameters.

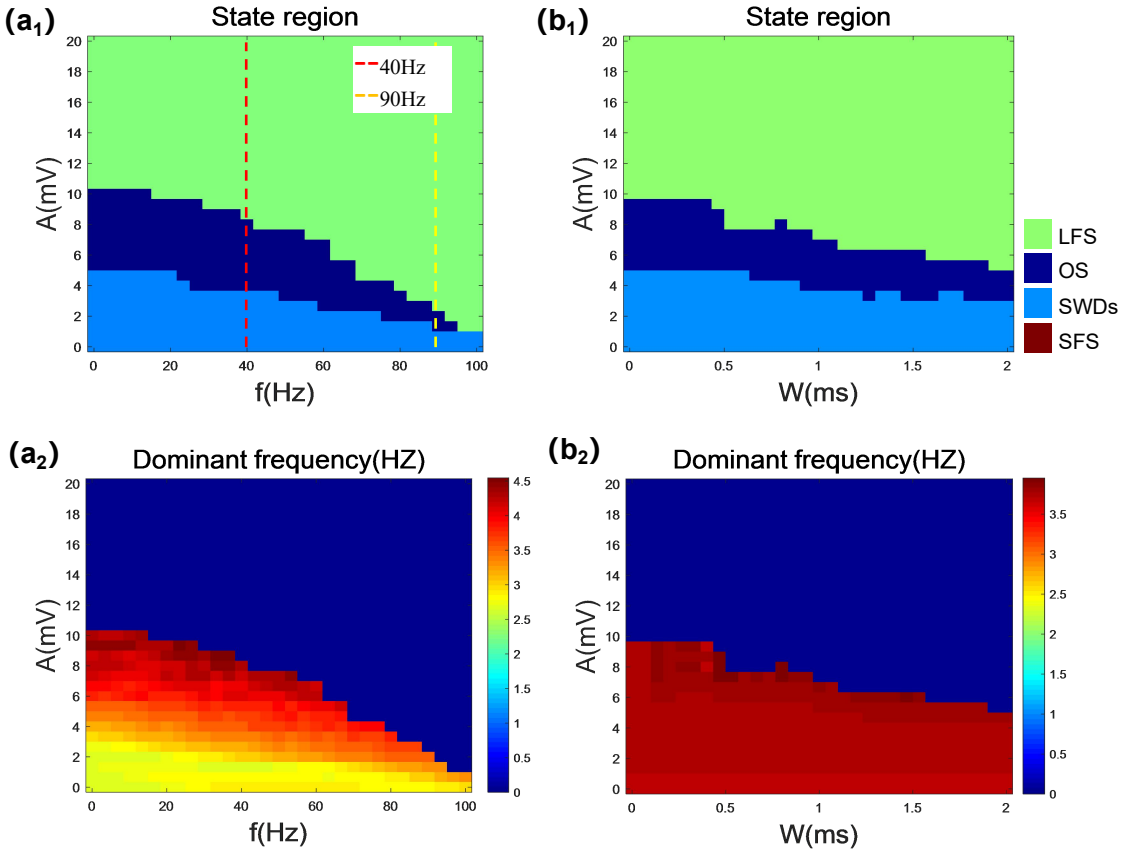


**Figure 11.** State and frequency diagrams of the FPS modulate SWDs based on different pulse widths ($W$) and frequencies ($f$) for the uniform amplitude parameter $A$. ($a_1$) State analysis on a two-dimensional plane ($f$, $A$), with a pulse width of $W = 1$ ms. Two dashed lines represent the positions at frequencies of 40 Hz and 90 Hz. ($b_1$) State analysis on a two-dimensional plane ($W$, $A$), with a frequency of $f = 50$ Hz. ($a_2$) and ($b_2$) are the corresponding main frequency analysis diagrams for ($a_1$) and ($b_1$), respectively. Here, $A = A_1 = A_2 = A_3 = A_4$, with a stimulation intensity of $v_{stim} = 0.785$ mV s.

The stimulation pattern we proposed achieves control over the system state by adjusting the stimulation parameters, which are initially undetermined. Through a multidimensional analysis of $A$, $f$, and $W$, this study systematically explores the impact of each parameter on the state transitions and roughly identifies a reasonable range for these parameters. For example, $A$ is the dominant parameter: an increase in $A$ directly drives the system to transition from the SWDs to either the OS or the LFS. $f$ and $W$ are auxiliary parameters: within specific ranges, fine-tuning these parameters further optimizes the state transition effects. Through a step-by-step exploration, the parameter range was gradually narrowed, and ultimately led to the identification of a reasonable combination of stimulation

parameters. However, there is room for improvement in the following areas: although $A$ is the key parameter, whether nonlinear interactions exist between $f$ and $W$ requires further verification. The obtained parameter range may depend on the initial conditions of the model, and the impact of different parameters on the model's generalizability needs to be considered.

## 5. Conclusions

This study systematically investigated the mechanisms of absence seizures and its control strategies using an improved BGCT mean-field model. Notably, we computationally validated the crucial regulatory role of the newly discovered STN-D direct projection pathway in controlling SWDs. Our findings demonstrated that enhancing this excitatory pathway effectively suppressed abnormal electrical activity by increasing the striatal activation, thus facilitating the transition from pathological states to normal rhythms or resting states. A further analysis revealed a significant correlation between the excitatory coupling strength of the STN-D pathway and system state transitions. Strengthening this coupling not only reduces striatal firing rates but also effectively suppresses abnormal synchronization in the corticothalamic network, thus offering fresh perspectives to control absence seizures. Interestingly, we observed synergistic effects between the STN-D pathway and other direct input pathways (EPN-D, SRN-D), thus revealing cascade network reactions that open new avenues to optimize seizure regulation strategies. The results showed that among the four main regulatory pathways (STN-D, EPN-D, SRN-D, D-D), the STN-D and EPN-D exhibited the most prominent SWD suppression, followed by the SRN-D, while the D-D showed limited effectiveness.

The breakthrough of this research lies in the innovative proposal of a novel stimulation paradigm (FPS). Through simulating parameter combinations, we confirmed that this paradigm could both replace the original striatal input and precisely modulate the SWD states. Specifically, enhancing excitatory projections such as the STN-D or appropriately adjusting external stimulation parameters (amplitude, frequency, pulse width) significantly suppressed the SWDs, ultimately converting pathological states to normal rhythms. By comparing the effects of four-phase pulse stimulation and the original striatal input on the basal ganglia-corticalthalamic mean-field model, this study aimed to provide a deeper understanding of the regulatory mechanisms of neural networks, thus offering new perspectives and insights for research in the field of neuroscience. The results indicated that this stimulation pattern successfully replaced the original striatal input and effectively controlled absence seizures. These findings not only provide theoretical support for a deeper understanding of the dynamic mechanisms of absence seizures but also offer important references to design novel neural stimulation methods to improve the treatment of epilepsy.

## Use of AI tools declaration

The authors declare they have not used Artificial Intelligence (AI) tools in the creation of this article.

## Acknowledgments

This work is supported by the National Natural Science Foundation of China (Grant No.12272002).

## Conflict of interest

Professor Lixia Duan is an editorial board member for Electronic Research Archive and was not involved in the editorial review and the decision to publish this article. The authors declare there is no conflict of interest.

## References


1. V. Crunelli, N. Leresche, Childhood absence epilepsy: genes, channels, neurons and networks, *Nat. Rev. Neurosci.*, **3** (2002), 371–382. https://doi.org/10.1038/nrn811
2. D. J. Thurman, E. Beghi, C. E. Begley, A. T. Berg, J. R. Buchhalter, D. Ding, et al., Standards for epidemiologic studies and surveillance of epilepsy, *Epilepsia*, **52** (2011), 2–26. https://doi.org/10.1111/j.1528-1167.2011.03121.x
3. M. Avoli, A brief history on the oscillating roles of thalamus and cortex in absence seizures, *Epilepsia*, **53** (2012), 779–789. https://doi.org/ 10.1111/j.1528-1167.2012.03421.x
4. J. A. Roberts, P. A. Robinson, Modeling absence seizure dynamics: implications for basic mechanisms and measurement of thalamocortical and corticothalamic latencies, *J. Theor. Biol.*, **253** (2008), 189–201. https://doi.org/10.1016/j.jtbi.2008.03.005
5. S. Rodrigues, D. Barton, R. Szalai, O. Benjamin, M. P. Richardson, J. R. Terry, Transitions to spike-wave oscillations and epileptic dynamics in a human cortico-thalamic mean-field model, *J. Comput. Neurosci.*, **27** (2009), 507–526. https://doi.org/10.1007/s10827-009-0166-2
6. V. Tancredi, G. Biagini, M. D'Antuono, J. Louvel, R. Pumain, M. Avoli, Spindle-like thalamocortical synchronization in a rat brain slice preparation, *J. Neurophysiol.*, **84** (2000), 1093–1097. https://doi.org/10.1152/jn.2000.84.2.1093
7. G. D'Arcangelo, M. D'Antuono, G. Biagini, R. Warren, V. Tancredi, M. Avoli, Thalamocortical oscillations in a genetic model of absence seizures, *Eur. J. Neurosci.*, **16** (2002), 2383–2393. https://doi.org/10.1046/j.1460-9568.2002.02411.x
8. T. Arakaki, S. Mahon, S. Charpier, A. Leblois, D. Hansel, The role of striatal feedforward inhibition in the maintenance of absence seizures, *J. Neurosci.*, **36** (2016), 9618–9632. https://doi.org/10.1523/JNEUROSCI.0208-16.2016
9. M. Chen, D. Guo, T. Wang, W. Jing, Y. Xia, P. Xu, et al., Bidirectional control of absence seizures by the basal ganglia: a computational evidence, *PLoS Comput. Biol.*, **10** (2014), e1003495. https://doi.org/10.1371/journal.pcbi.1003495
10. C. Deransart, L. Vercueil, C. Marescaux, A. Depaulis, The role of basal ganglia in the control of generalized absence seizures, *Epilepsy Res.*, **32** (1998), 213–223. https://doi.org/10.1016/s0920-1211(98)00053-9
11. D. Fan, Q. Wang, Improved control effect of absence seizures by autaptic connections to the subthalamic nucleus, *Phys. Rev. E*, **98** (2018), 052414. https://doi.org/10.1103/PhysRevE.98.052414
12. B. Hu, D. Guo, Q. Wang, Control of absence seizures induced by the pathways connected to SRN in corticothalamic system, *Cognit. Neurodyn.*, **9** (2015), 279–289. https://doi.org/10.1007/s11571-014-9321-1

13. B. Hu, Q. Wang, Controlling absence seizures by deep brain stimulus applied on substantia nigra pars reticulata and cortex, *Chaos, Solitons Fractals*, **80** (2015), 13–23. https://doi.org/10.1016/j.chaos.2015.02.014

14. C. Luo, Q. Li, Y. Xia, X. Lei, K. Xue, Z. Yao, et al., Resting state basal ganglia network in idiopathic generalized epilepsy, *Hum. Brain Mapp.*, **33** (2012), 1279–1294. https://doi.org/10.1002/hbm.21286

15. J. Vuong, A. Devergnas, The role of the basal ganglia in the control of seizure, *J. Neural Transm.*, **125** (2018), 531–545. https://doi.org/10.1007/s00702-017-1768-x

16. A. Saunders, I. A. Oldenburg, V. K. Berezovskii, C. A. Johnson, N. D. Kingery, H. L. Elliott, et al., A direct GABAergic output from the basal ganglia to frontal cortex, *Nature*, **521** (2015), 85–89. https://doi.org/10.1038/nature14179

17. M. Chen, D. Guo, M. Li, T. Ma, S. Wu, J. Ma, et al., Critical roles of the direct GABAergic pallidocortical pathway in controlling absence seizures, *PLoS Comput. Biol.*, **11** (2015), e1004539. https://doi.org/10.1371/journal.pcbi.1004539

18. M. Chen, Y. Zhu, R. Yu, Y. Hu, H. Wan, R. Zhang, et al., Insights on the role of external globus pallidus in controlling absence seizures, *Neural Networks*, **135** (2021), 78–90. https://doi.org/10.1016/j.neunet.2020.12.006

19. B. Hu, W. Zhou, X. Ma, Striatum is the potential target for treating absence epilepsy: a theoretical evidence, *Cognit. Neurodyn.*, **18** (2024), 3775–3790. https://doi.org/10.1007/s11571-024-10161-6

20. X. Wang, L. Yin, Y. Yu, Q. Wang, Unraveling the dynamical mechanisms of motor preparation based on the heterogeneous attractor model, *Chaos, Solitons Fractals*, **194** (2025), 116220. https://doi.org/10.1016/j.chaos.2025.116220

21. A. Saunders, K. W. Huang, B. L. Sabatini, Globus pallidus externus neurons expressing parvalbumin interconnect the subthalamic nucleus and striatal interneurons, *PLoS One*, **11** (2016), e0149798. https://doi.org/10.1371/journal.pone.0149798

22. K. Kondabolu, N. M. Doig, O. Ayeko, B. Khan, A. Torres, D. Calvigioni, et al., A selective projection from the subthalamic nucleus to parvalbumin-expressing interneurons of the striatum, *eNeuro*, **10** (2023), ENEURO.0417–21.2023. https://doi.org/10.1523/ENEURO.0417-21.2023

23. D. Masur, S. Shinnar, A. Cnaan, R. C. Shinnar, P. Clark, J. Wang, et al., Pretreatment cognitive deficits and treatment effects on attention in childhood absence epilepsy, *Neurology*, **81** (2013), 1572–1580. https://doi.org/10.1212/WNL.0b013e3182a9f3ca

24. P. Kwan, A. Arzimanoglou, A. T. Berg, M. J. Brodie, W. Allen Hauser, G. Mathern, et al., Definition of drug resistant epilepsy: consensus proposal by the ad hoc Task Force of the ILAE Commission on Therapeutic Strategies, *Epilepsia*, **51** (2010), 1069–1077. https://doi.org/10.1111/j.1528-1167.2009.02397.x

25. X. Tan, H. Zhang, Y. Xie, Y. Chai, Electromagnetic radiation and electrical stimulation controls of absence seizures in a coupled reduced corticothalamic model, *Electron. Res. Arch.*, **31** (2023), 58–74. https://doi.org/10.3934/era.2023004

26. D. Fan, Y. Wang, J. Wu, S. Hou, Q. Wang, The preview control of a corticothalamic model with disturbance, *Electron. Res. Arch.*, **32** (2024), 812–835. https://doi.org/10.3934/era.2024039

27. X. Zhu, Y. Liu, S. Huang, R. Li, Y. Chai, Modulation of epileptiform discharges by heterogeneous interneurons and external stimulation strategies in the thalamocortical model, *Electron. Res. Arch.*, **33** (2025), 2391–2411. https://doi.org/10.3934/era.2025106

28. A. Fasano, A. Daniele, A. Albanese, Treatment of motor and non-motor features of Parkinson's disease with deep brain stimulation, *Lancet Neurol.*, **11** (2012), 429–442. https://doi.org/10.1016/S1474-4422(12)70049-2

29. A. L. Benabid, S. Chabardes, J. Mitrofanis, P. Pollak, Deep brain stimulation of the subthalamic nucleus for the treatment of Parkinson's disease, *Lancet Neurol.*, **8** (2009), 67–81. https://doi.org/10.1016/S1474-4422(08)70291-6

30. D. Fan, Y. Zheng, Z. Yang, Q. Wang, Improving control effects of absence seizures using single-pulse alternately resetting stimulation (SARS) of corticothalamic circuit, *Appl. Math. Mech.*, **41** (2020), 1287–1302. https://doi.org/10.1007/s10483-020-2644-8

31. H. S. Haghighi, A. H. D. Markazi, Control of epileptic seizures by electrical stimulation: A model-based study, *Biomed. Phys. Eng. Express*, **7** (2021), 065009. https://doi.org/10.1088/2057-1976/ac240d

32. B. J. Stieve, T. J. Richner, C. Krook-Magnuson, T. I. Netoff, E. Krook-Magnuson, Optimization of closed-loop electrical stimulation enables robust cerebellar-directed seizure control, *Brain*, **146** (2023), 91–108. https://doi.org/10.1093/brain/awac051

33. B. Hu, J. Zhao, Y. Ao, X. Cai, The possible role of electromagnetic induction in the regulation of absence seizures: evidence from a computational model, *Nonlinear Dyn.*, **113** (2025), 2711–2728. https://doi.org/10.1007/s11071-024-10345-z

34. S. Hou, D. Fan, Q. Wang, Regulating absence seizures by tri-phase delay stimulation applied to globus pallidus internal, *Appl. Math. Mech.*, **43** (2022), 1399–1414. https://doi.org/10.1007/s10483-022-2896-7

35. C. He, D. Fan, W. Wang, Q. Wang, G. Baier, Network dynamics mechanisms underlying the instigation and propagation of cortical spreading depression, *Neurocomputing*, **649** (2025), 130733. https://doi.org/10.1016/j.neucom.2025.130733

36. J. Zhao, Q. Wang, Y. Yu, A new pathway for controlling absence seizures by reducing GABA uptake from astrocytes: a dynamical perspective, *Commun. Nonlinear Sci. Numer. Simul.*, **149** (2025), 108929. https://doi.org/10.1016/j.cnsns.2025.108929

37. J. T. Paz, M. Chavez, S. Saillet, J. M. Deniau, S. Charpier, Activity of ventral medial thalamic neurons during absence seizures and modulation of cortical paroxysms by the nigrothalamic pathway, *J. Neurosci.*, **27** (2007), 929–941. https://doi.org/10.1523/JNEUROSCI.4677-06.2007

38. S. J. van Albada, P. A. Robinson, Mean-field modeling of the basal ganglia-thalamocortical system. I: Firing rates in healthy and parkinsonian states, *J. Theor. Biol.*, **257** (2009), 642–663. https://doi.org/10.1016/j.jtbi.2008.12.018

39. S. J. van Albada, R. T. Gray, P. M. Drysdale, P. A. Robinson, Mean-field modeling of the basal ganglia-thalamocortical system. II: Dynamics of parkinsonian oscillations, *J. Theor. Biol.*, **257** (2009), 664–688. https://doi.org/10.1016/j.jtbi.2008.12.013

40. P. A. Robinson, C. J. Rennie, D. L. Rowe, Dynamics of large-scale brain activity in normal arousal states and epileptic seizures, *Phys. Rev. E*, **65** (2002), 041924. https://doi.org/10.1103/PhysRevE.65.041924

41. M. Breakspear, J. A. Roberts, J. R. Terry, S. Rodrigues, N. Mahant, P. A. Robinson, A unifying explanation of primary generalized seizures through nonlinear brain modeling and bifurcation analysis, *Cereb. Cortex*, **16** (2006), 1296–1313. https://doi.org/10.1093/cercor/bhj072

42. C. C. Chiang, C. C. Lin, M. S. Ju, D. M. Durand, High frequency stimulation can suppress globally seizures induced by 4-AP in the rat hippocampus: an acute in vivo study, *Brain Stimul.*, **6** (2013), 180–189. https://doi.org/10.1016/j.brs.2012.04.008


AIMS Press